

Active Constraints using Vector Field Inequalities for Surgical Robots

Murilo M. Marinho, *Student Member, IEEE*, Bruno V. Adorno, *Senior Member, IEEE*,
Kanako Harada, *Member, IEEE*, and Mamoru Mitsuishi, *Member, IEEE*

Abstract—Robotic assistance allows surgeons to perform dexterous and tremor-free procedures, but is still underrepresented in deep brain neurosurgery and endonasal surgery where the workspace is constrained. In these conditions, the vision of surgeons is restricted to areas near the surgical tool tips, which increases the risk of unexpected collisions between the shafts of the instruments and their surroundings, in particular in areas outside the surgical field-of-view. Active constraints can be used to prevent the tools from entering restricted zones and thus avoid collisions. In this paper, a vector field inequality is proposed that guarantees that tools do not enter restricted zones. Moreover, in contrast with early techniques, the proposed method limits the tool approach velocity in the direction of the forbidden zone boundary, guaranteeing a smooth behavior and that tangential velocities will not be disturbed. The proposed method is evaluated in simulations featuring two eight degrees-of-freedom manipulators that were custom-designed for deep neurosurgery. The results show that both manipulator-manipulator and manipulator-boundary collisions can be avoided using the vector field inequalities.

I. INTRODUCTION

Surgical robots have received considerable attention in the context of minimally invasive surgery, as aids in procedures performed through small incisions, in systems such as the da Vinci, the RAVEN [1], and the SteadyHand [2]. Their use has been extended to procedures in restricted workspaces such as deep brain microsurgery [3], [4] and endonasal surgery [5].

In minimally invasive surgery and microsurgery, the surgeon operates with long thin tools, and views the workspace through an endoscope or microscope. Their vision is frequently limited to a region near the surgical tool tips. As the surgeon operates the tools, the tool shaft may inadvertently collide with neighboring structures. In particular in microsurgery, the amplitude of hand tremor can be higher than size of the structures being treated. In this context, surgical robots are used as equipment to assist the surgeon in order to increase accuracy and safety, and reduce surgeon's mental load and the effects of their hand tremor.

This work was funded by the ImPACT Program of the Council for Science, Technology and Innovation (Cabinet Office, Government of Japan). Murilo M. Marinho has been supported by the Japanese Ministry of Education, Culture, Sports, Science, and Technology (MEXT). Bruno V. Adorno has been supported by the Brazilian agencies CAPES, CNPq, FAPEMIG, and by the project INCT (National Institute of Science and Technology) under the grant CNPq (Brazilian National Research Council) 465755/2014-3, FAPESP (São Paulo Research Foundation)2014/50851-0.

Murilo M. Marinho, Kanako Harada, and Mitsuishi Mamoru are with Department of Mechanical Engineering, the University of Tokyo, Tokyo, Japan. Email: {murilo, kanako, mamoru}@nml.t.u-tokyo.ac.jp. Bruno V. Adorno is with the Department of Electrical Engineering and with the Graduate Program in Electrical Engineering - Federal University of Minas Gerais, Belo Horizonte-MG, Brazil. Email: adorno@ufmg.br.

To increase accuracy and attenuate hand tremor, surgical robots are commanded in task space coordinates either through teleoperation or comanipulation. Joint space control inputs are generally obtained by using a kinematic control law, which is usually based on the robot differential kinematics [6]. Kinematic control laws are valid when low accelerations are imposed in the joint space, and are ubiquitous in control algorithms designed for surgical robotics [5], [7]–[10], since low accelerations are expected in such scenarios.

An increase in safety and a reduction in the surgeon's mental load has been achieved through the generation of active constraints (virtual fixtures) that can, for instance, act as a layer of safety to prevent the surgical tool from entering a restricted region, even if this contradicts the commands given to the robot [5], [7], or transparently generate constrained motion [8]–[10]. An in-depth survey of active constraints was presented by Bowyer *et al.* [11]. More recent papers published after this survey addressed the use of guidance virtual fixtures to assist in knot tying in robotic laparoscopy [12], and to allow surgeons to feel the projected force feedback from the distal end of a tool to the proximal end of a tool in a comanipulation context [13].

The generation of active constraints using kinematic control laws requires obtaining a Jacobian that relates the constraint to the task at hand. For instance, for the generation of the remote center of motion in minimally invasive surgery, some groups [8], [9] developed Jacobians to maintain a low remote center of motion error. Aghakhani *et al.* [8] constrained lateral motion in the pivoting point by using the pivoting point dynamics, and Pham *et al.* [9] used the so-called constrained Jacobian to project the desired end effector velocity into a constrained velocity in the pivoting point frame. Additional requirements, such as the desired tool tip pose following and obstacle avoidance are usually projected in the null space of the constrained task or stacked to form an augmented Jacobian. The main problem from which both approaches suffer is the difficulty in adding inequality constraints, which are useful in the design of virtual fixtures [14].

II. RELATED WORKS

A framework for manipulator control in surgical robotics that can take inequalities into account was developed by Funda *et al.* [14] using quadratic programming. Their framework was extended by Kapoor *et al.* [7], who developed a library of virtual fixtures, including five task primitives that can be combined into customized active constraints. Li *et al.* [5] used the extended framework to aid operators to

move a surgical tool in a highly constrained space in sinus surgery without collisions. In all these studies, non-linear constraints were used. Solving for non-linear constraints requires an initial guess and takes longer than solving for linear constraints, and therefore, the authors also considered the use of linear *approximations*, which reduce computation time but may result in errors [7]. This raises the question of whether the constraints can be written directly in linear form, avoiding approximations. An additional consideration is that the closed-loop stability of their approach has never been formally proven.

Gonçalves *et al.* [15] developed a Lyapunov-stable kinematic controller that takes into account both equality and inequality constraints, which are linear with respect to the joint velocities. They experimentally validated their approach using a humanoid robot. Their framework was extended by Quiroz-Omana and Adorno [16] to the control of a mobile manipulator by adding a unilateral equality constraint that pushes the mobile manipulator out of a forbidden zone. This, however, was a reactive constraint and did not impede the mobile robot from entering the restricted zone in the first place. Such reactive behavior is particularly undesirable in medical robotic applications, in which the patient may be harmed if a tool enters a forbidden zone.

It is important to note that, in prior approaches [5], [7], [14], when the tool reaches a restricted zone boundary the obstacle constraint is suddenly activated, which might cause the robot to show acceleration peaks. Researchers attempted to address this issue. For instance, Xia *et al.* [17] reduced the proportional gain in an admittance control law proportionally to the distance between the robot and the nearest obstacle. This allowed the system to smoothly avoid collisions, but also impeded motion tangential to the obstacle boundary. Prada and Payandeh [18] proposed adding a time-varying gain to smooth the attraction force of attractive virtual fixtures.

A. Statement of contributions

In this paper, we propose a new concept of vector field inequality applied to active constraints that further extends the developments of Gonçalves *et al.* [15] and Quiroz-Omana and Adorno [16]. The proposed vector field inequality allows the designer to set a maximum approach speed in the direction of the restriction boundaries, which guarantees that the robot can smoothly approach restricted zones without trespassing on their limits, and that the velocities orthogonal to the restriction boundaries are undisturbed.

Moreover, in this study we also developed a set of control primitives for restricted zones, including point, plane, line, and cylinder relations, which can be customized to model complex environments and interactions. The effectiveness of the proposed approach is shown in realistic simulated experiments.

The current work was conducted in the context of *Project 2: Smart Arm*, part of the *ImPACT Bionic Humanoids Propelling New Industrial Revolution* project, the objective

of which is to develop robotic systems and control frameworks to allow robot-aided surgical procedures in constrained spaces, such as those involved in transnasal pituitary gland resection and surgeries in deep and narrow regions of the brain.

III. MATHEMATICAL BACKGROUND

The proposed virtual fixtures framework extensively uses dual quaternion algebra because of its several advantages over other representations. For instance, unit dual quaternions do not have representational singularities and are more compact and computationally efficient than homogeneous transformation matrices [19]. Moreover, their strong algebraic properties allow different robots to be systematically modeled [16], [19]–[21] and, in addition to representing rigid motions, dual quaternion algebra is very useful for describing twists, wrenches, and several geometrical primitives—e.g., Plücker lines and planes—in very straightforwardly [22]. The next subsection introduces the basic definitions of quaternions and dual quaternions; more information can be found in [20], [22], [23].

A. Quaternions and dual Quaternions

Quaternions can be regarded as an extension of complex numbers. The quaternion set is defined as

$$\mathbb{H} \triangleq \left\{ h_1 + \hat{i}h_2 + \hat{j}h_3 + \hat{k}h_4 : h_1, h_2, h_3, h_4 \in \mathbb{R} \right\},$$

in which the imaginary units \hat{i} , \hat{j} , and \hat{k} have the properties $\hat{i}^2 = \hat{j}^2 = \hat{k}^2 = \hat{i}\hat{j}\hat{k} = -1$. The dual quaternion set is defined as

$$\mathcal{H} \triangleq \left\{ \mathbf{h} + \varepsilon \mathbf{h}' : \mathbf{h}, \mathbf{h}' \in \mathbb{H}, \varepsilon^2 = 0, \varepsilon \neq 0 \right\},$$

where ε is the dual (or Clifford) unit [23]. Addition and multiplication are defined for dual quaternions analogously to complex numbers, and hence we need only to respect the properties of the imaginary and dual units.

Given $\underline{\mathbf{h}} \in \mathcal{H}$ such that $\underline{\mathbf{h}} = h_1 + \hat{i}h_2 + \hat{j}h_3 + \hat{k}h_4 + \varepsilon (h'_1 + \hat{i}h'_2 + \hat{j}h'_3 + \hat{k}h'_4)$, we define the operators

$$\mathcal{P}(\underline{\mathbf{h}}) \triangleq h_1 + \hat{i}h_2 + \hat{j}h_3 + \hat{k}h_4, \quad \mathcal{D}(\underline{\mathbf{h}}) \triangleq h'_1 + \hat{i}h'_2 + \hat{j}h'_3 + \hat{k}h'_4,$$

and

$$\text{Re}(\underline{\mathbf{h}}) \triangleq h_1 + \varepsilon h'_1,$$

$$\text{Im}(\underline{\mathbf{h}}) \triangleq \hat{i}h_2 + \hat{j}h_3 + \hat{k}h_4 + \varepsilon (\hat{i}h'_2 + \hat{j}h'_3 + \hat{k}h'_4).$$

The conjugate of $\underline{\mathbf{h}}$ is defined as $\underline{\mathbf{h}}^* \triangleq \text{Re}(\underline{\mathbf{h}}) - \text{Im}(\underline{\mathbf{h}})$, and its norm is given by $\|\underline{\mathbf{h}}\| = \sqrt{\underline{\mathbf{h}}\underline{\mathbf{h}}^*} = \sqrt{\underline{\mathbf{h}}^*\underline{\mathbf{h}}}$.

The set $\mathbb{H}_p \triangleq \{\mathbf{h} \in \mathbb{H} : \text{Re}(\mathbf{h}) = 0\}$ is isomorphic to \mathbb{R}^3 under the addition operation. Thus, the quaternion $(x\hat{i} + y\hat{j} + z\hat{k}) \in \mathbb{H}_p$ represents the point $(x, y, z) \in \mathbb{R}^3$.

The set of quaternions with unit norm is defined as $\mathbb{S}^3 \triangleq \{\mathbf{h} \in \mathbb{H} : \|\mathbf{h}\| = 1\}$, and $\mathbf{r} \in \mathbb{S}^3$ can always be written as $\mathbf{r} = \cos(\phi/2) + \mathbf{v} \sin(\phi/2)$, where $\phi \in \mathbb{R}$ is the rotation angle around the rotation axis $\mathbf{v} \in \mathbb{S}^3 \cap \mathbb{H}_p$ [22]. Elements of the set $\mathcal{S} \triangleq \{\underline{\mathbf{h}} \in \mathcal{H} : \|\underline{\mathbf{h}}\| = 1\}$ are called unit dual quaternions and represent tridimensional poses (i.e.,

combined position and orientation) of rigid bodies. Given $\underline{x} \in \underline{\mathcal{S}}$, it can always be written as $\underline{x} = \mathbf{r} + \varepsilon(1/2) \mathbf{t} \mathbf{r}$, where $\mathbf{r} \in \mathbb{S}^3$ and $\mathbf{t} \in \mathbb{H}_p$ represent the orientation and position, respectively [23]. The set $\underline{\mathcal{S}}$ equipped with the multiplication operation forms the group $\text{Spin}(3) \rtimes \mathbb{R}^3$, which double covers $\text{SE}(3)$.

Elements of the set $\mathcal{H}_p \triangleq \{\underline{\mathbf{h}} \in \mathcal{H} : \text{Re}(\underline{\mathbf{h}}) = 0\}$ are called pure dual quaternions and are useful for representing Plücker lines. More specifically, a Plücker line belongs to the set $\mathcal{H}_p \cap \underline{\mathcal{S}}$ and thus is represented by a pure unit dual quaternion such as [20], [22]

$$\underline{\mathbf{l}} = \mathbf{l} + \varepsilon \mathbf{m}, \quad (1)$$

where $\mathbf{l} \in \mathbb{H}_p \cap \mathbb{S}^3$ is a pure quaternion with unit norm that represents the line direction, and the line moment is given by $\mathbf{m} = \mathbf{p}_l \times \mathbf{l}$, in which $\mathbf{p}_l \in \mathbb{H}_p$ is a point in the line and \times is the cross product. Given $\underline{\mathbf{a}}, \underline{\mathbf{b}} \in \mathcal{H}_p$, the inner product and the cross product are respectively defined as [20], [22]

$$\langle \underline{\mathbf{a}}, \underline{\mathbf{b}} \rangle \triangleq -\frac{\underline{\mathbf{a}}\underline{\mathbf{b}} + \underline{\mathbf{b}}\underline{\mathbf{a}}}{2}, \quad \underline{\mathbf{a}} \times \underline{\mathbf{b}} \triangleq \frac{\underline{\mathbf{a}}\underline{\mathbf{b}} - \underline{\mathbf{b}}\underline{\mathbf{a}}}{2}. \quad (2)$$

The operator vec_4 maps quaternions into \mathbb{R}^4 and vec_8 maps dual quaternions into \mathbb{R}^8 . For instance, $\text{vec}_4 \mathbf{h} = [h_1 \ h_2 \ h_3 \ h_4]^T$ and $\text{vec}_8 \underline{\mathbf{h}} = [h_1 \ h_2 \ h_3 \ h_4 \ h'_1 \ h'_2 \ h'_3 \ h'_4]^T$.

Finally, given $\mathbf{h}_1, \mathbf{h}_2 \in \mathbb{H}$, the Hamilton operators are matrices that satisfy $\text{vec}_4(\mathbf{h}_1 \mathbf{h}_2) = \overset{+}{\mathbf{H}}_4(\mathbf{h}_1) \text{vec}_4 \mathbf{h}_2 = \overset{-}{\mathbf{H}}_4(\mathbf{h}_2) \text{vec}_4 \mathbf{h}_1$. Analogously, given $\underline{\mathbf{h}}_1, \underline{\mathbf{h}}_2 \in \mathcal{H}$, the Hamilton operators satisfy $\text{vec}_8(\underline{\mathbf{h}}_1 \underline{\mathbf{h}}_2) = \overset{+}{\mathbf{H}}_8(\underline{\mathbf{h}}_1) \text{vec}_8 \underline{\mathbf{h}}_2 = \overset{-}{\mathbf{H}}_8(\underline{\mathbf{h}}_2) \text{vec}_8 \underline{\mathbf{h}}_1$ [22].

It can be shown by direct calculation that, when $\mathbf{a}, \mathbf{b} \in \mathbb{H}_p$, the inner product can be written as

$$\langle \mathbf{a}, \mathbf{b} \rangle = (\text{vec}_4 \mathbf{a})^T \text{vec}_4 \mathbf{b} = (\text{vec}_4 \mathbf{b})^T \text{vec}_4 \mathbf{a}$$

and the cross product between \mathbf{a} and \mathbf{b} , which is analogous to the case of vectors in \mathbb{R}^3 , can be mapped into \mathbb{R}^4 by using the operator $\overline{\mathbf{S}}(\cdot)$ as

$$\begin{aligned} \text{vec}_4(\mathbf{a} \times \mathbf{b}) &= \underbrace{\begin{bmatrix} 0 & 0 & 0 & 0 \\ 0 & 0 & -a_4 & a_3 \\ 0 & a_4 & 0 & -a_2 \\ 0 & -a_3 & a_2 & 0 \end{bmatrix}}_{\overline{\mathbf{S}}(\mathbf{a})} \text{vec}_4 \mathbf{b} \\ &= \overline{\mathbf{S}}(\mathbf{a}) \text{vec}_4 \mathbf{b} = \overline{\mathbf{S}}(\mathbf{b})^T \text{vec}_4 \mathbf{a}. \end{aligned}$$

Finally, the time-derivative of a quaternion $\mathbf{a} \in \mathbb{H}_p$ is given by

$$\frac{d(\|\mathbf{a}\|)}{dt} = \frac{\dot{\mathbf{a}}\mathbf{a}^* + \mathbf{a}\dot{\mathbf{a}}^*}{2\|\mathbf{a}\|} = \frac{\langle \dot{\mathbf{a}}, \mathbf{a} \rangle}{\|\mathbf{a}\|} = \frac{1}{\|\mathbf{a}\|} \text{vec}_4 \mathbf{a}^T \text{vec}_4 \dot{\mathbf{a}}, \quad (3)$$

since for any $\mathbf{a} \in \mathbb{H}_p$ we have $\mathbf{a}^* = -\mathbf{a}$.

B. Differential kinematics

Differential kinematics is the relation between task space velocities and joint space velocities, in the general form $\dot{\mathbf{x}} = \mathbf{J}\dot{\mathbf{q}}$, in which $\dot{\mathbf{x}} \in \mathbb{R}^m$ is the vector of task space velocities, $\dot{\mathbf{q}} \in \mathbb{R}^n$ is the vector of manipulator joint velocities, and $\mathbf{J} \in \mathbb{R}^{m \times n}$ is the Jacobian matrix.

For instance, given the robot end effector pose $\underline{\mathbf{x}} \triangleq \underline{\mathbf{x}}(\mathbf{q}(t)) \in \text{Spin}(3) \rtimes \mathbb{R}^3$, the differential kinematics is given by $\text{vec}_8 \dot{\underline{\mathbf{x}}} = \mathbf{J}_{\underline{\mathbf{x}}}\dot{\mathbf{q}}$, where $\mathbf{J}_{\underline{\mathbf{x}}} \in \mathbb{R}^{8 \times n}$ is the dual quaternion analytical Jacobian, which can be found by using dual quaternion algebra [19]. Similarly, given the end effector position $\underline{\mathbf{t}} \triangleq \underline{\mathbf{t}}(\mathbf{q}(t)) \in \mathbb{H}_p$ and the orientation $\mathbf{r} \triangleq \mathbf{r}(\mathbf{q}(t)) \in \mathbb{S}^3$, we have

$$\text{vec}_4 \dot{\underline{\mathbf{t}}} = \mathbf{J}_t \dot{\mathbf{q}}, \quad (4)$$

$$\text{vec}_4 \dot{\mathbf{r}} = \mathbf{J}_r \dot{\mathbf{q}}, \quad (5)$$

where $\mathbf{J}_t, \mathbf{J}_r \in \mathbb{R}^{4 \times n}$ are calculated from $\mathbf{J}_{\underline{\mathbf{x}}}$ also by using dual quaternion algebra [24]. It is important to note that, in general applications, $\underline{\mathbf{x}}, \underline{\mathbf{t}}$, and \mathbf{r} may refer to any relevant coordinate system related to the robot, and not only to the end effector.

C. Linear programming for differential inverse kinematics

In closed-loop differential inverse kinematics, first a desired task space target, \mathbf{x}_d , and the task error $\tilde{\mathbf{x}} = \mathbf{x} - \mathbf{x}_d$ are defined. For $\eta \in (0, \infty)$, the minimum-norm analytical solution of the optimization problem

$$\min_{\dot{\mathbf{q}}} \|\mathbf{J}\dot{\mathbf{q}} + \eta\tilde{\mathbf{x}}\|_2^2 \quad (6)$$

is $\mathbf{J}^\dagger \eta \tilde{\mathbf{x}} = \dot{\mathbf{q}}$, in which \mathbf{J}^\dagger is the generalized Moore-Penrose pseudoinverse of \mathbf{J} .

Adding inequality and equality constraints in Problem 6 turns it into a quadratic programming problem requiring a numerical solver [25]. The 1-norm analogue of Problem 6 is

$$\min_{\dot{\mathbf{q}}} \|\mathbf{J}\dot{\mathbf{q}} + \eta\tilde{\mathbf{x}}\|_1. \quad (7)$$

A Lyapunov stable solution for Problem 7 that considers both equality and inequality constraints is given by the following linear program in canonical form [15],

$$\begin{aligned} &\min_{\mathbf{g}} [-\mathbf{1}^T \mathbf{J} \ \mathbf{1}^T \mathbf{J} \ \mathbf{2} \cdot \mathbf{1}^T \ \mathbf{0}^T \ \mathbf{0}^T] \mathbf{g} - \eta \mathbf{1}^T \tilde{\mathbf{x}} \\ &\text{subject to} \begin{bmatrix} \mathbf{J} & -\mathbf{J} & -\mathbf{I} & \mathbf{I} & \mathbf{0} & \mathbf{0} \\ \mathbf{1}^T & \mathbf{1}^T & \mathbf{0}^T & \mathbf{0}^T & \mathbf{1} & \mathbf{0}^T \end{bmatrix} \mathbf{g} = \begin{bmatrix} -\eta\tilde{\mathbf{x}} \\ \beta \|\tilde{\mathbf{x}}\|_1 \\ \mathbf{w} \end{bmatrix}, \quad (8) \\ &\mathbf{g} \geq \mathbf{0} \end{aligned}$$

where $\mathbf{g} = [\dot{\mathbf{q}}_P^T \ \dot{\mathbf{q}}_N^T \ \mathbf{y}^T \ z_A^T \ z_B^T \ z_C^T]^T$ is the vector of decision variables. Moreover, $\mathbf{0}^T$ and $\mathbf{1}^T$ are row vectors of ones and zeros of appropriate dimensions, respectively. In the canonical form, all decision variables should be non-negative, and hence the joint velocities are split into the non-negative $\dot{\mathbf{q}}_P$ and $\dot{\mathbf{q}}_N$ such that

$$\dot{\mathbf{q}} = \dot{\mathbf{q}}_P - \dot{\mathbf{q}}_N. \quad (9)$$

Moreover, \mathbf{y} is a vector of residuals for the objective function, and the slack variables z_A, z_B , and z_C are used to transform inequality constraints into equality ones.

The matrix of constraints has three horizontal blocks from top to bottom. The first block concerns error convergence, the second block guarantees that the joints will stop moving when $\tilde{\mathbf{x}} \rightarrow 0$ with $\beta \in (0, \infty)$, and the third block is a generic block of r constraints, in which $\mathbf{W} \in \mathbb{R}^{r \times n}$ and \mathbf{w}

$\in \mathbb{R}^{r \times 1}$. The vector field inequalities proposed in this work concern an appropriate choice of \mathbf{W} and \mathbf{w} to generate active constraints, as described in the following section.

IV. VECTOR FIELD INEQUALITY

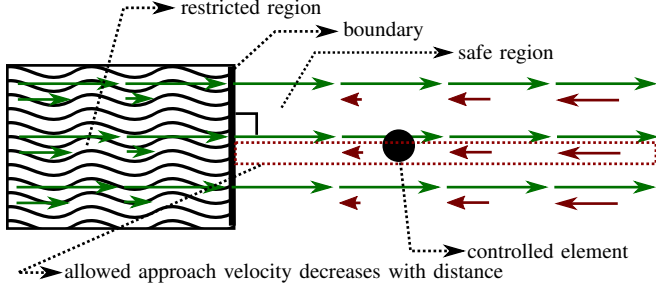


Fig. 1. Proposed vector field inequality method. The vector field is given by an inequality constraint, and to each point in space is assigned a maximum approach velocity (the red vector in each vector pair), and a maximum separating velocity (the green vector in each vector pair) in the direction perpendicular to the restricted zone boundary. Tangential velocities are unconstrained.

The vector field inequality proposed in this paper is a general method for active constraints. It requires:

- 1) A function $d(t) \in \mathbb{R}$ that encodes the (signed) distance between the two collidable entities, and
- 2) The Jacobian relating the time derivative of the distance and the joint velocities in the general form

$$\dot{d}(t) = \underbrace{\frac{\partial(d(t))}{\partial \mathbf{q}}}_{\mathbf{J}_d} \dot{\mathbf{q}}. \quad (10)$$

Using the distance function and the Jacobian, complex restricted zones can be generated, by either maintaining the distance above a desired level or keeping the distance below a certain level. The vector field inequality is illustrated in Fig. 1.

A. Preventing the robot from entering a restricted region

We first define a minimum safe distance, $d_{\text{safe}} \in [0, \infty)$, that delineates the boundary of the restricted zone. We then define a distance error as

$$\tilde{d}(t) \triangleq d(t) - d_{\text{safe}}, \quad (11)$$

which will be positive when in the safe-zone, zero along the boundary, and negative within the restricted zone.

Assuming a constant safe distance, the distance error dynamics is given by $\dot{\tilde{d}}(t) = \dot{d}(t)$. A positive $\tilde{d}(t)$ means that the system is moving away from the restricted space boundary and a negative $\tilde{d}(t)$ means that the system is moving closer to the restricted space. The goal is to constrain the distance dynamics by the inequality

$$\dot{\tilde{d}}(t) \geq -\eta_d \tilde{d}(t), \quad (12)$$

where $\eta_d \in (0, \infty)$.

To understand Constraint 12, let us suppose that $\tilde{d}(t) > 0$, which means that the system is outside the restricted

zone. In this situation, *any* increase in distance is *always* allowed, which implies $\dot{\tilde{d}} \geq 0 \geq -\eta_d \tilde{d}$. However, when the system is approaching the boundary from the safe region (i.e., $0 \geq \tilde{d} \geq -\eta_d \tilde{d}$), it can approach with a maximum velocity that decreases, in the worst case, exponentially with the distance $\tilde{d}(t)$, because the maximum decreasing rate is achieved when $\dot{\tilde{d}}(t) = -\eta_d \tilde{d}(t)$. Thus, the closer the object is to the boundary, the slower it can move in its direction. Any slower motion toward the boundary is also allowed, and hence $\dot{\tilde{d}}(t) \geq -\eta_d \tilde{d}(t)$. As soon as $\tilde{d}(t) = 0$, the restriction becomes $\dot{\tilde{d}}(t) \geq 0$ and therefore the system will not enter the restricted zone.

Considering (10), Constraint 12 is written explicitly in terms of joint velocities as

$$\mathbf{J}_d \dot{\mathbf{q}} \geq -\eta_d \tilde{d}(t) \iff -\mathbf{J}_d \dot{\mathbf{q}} \leq \eta_d \tilde{d}(t). \quad (13)$$

To turn Constraint 13 into an equality and fit it into the linear programming formalism, we introduce the slack variable z_D and decompose $\dot{\mathbf{q}}$ as in (9) to find

$$-\mathbf{J}_d \dot{\mathbf{q}}_P + \mathbf{J}_d \dot{\mathbf{q}}_N + z_D = \eta_d \tilde{d}(t). \quad (14)$$

Notice that any number of constraints in the form of Constraint 14 can be found for different interactions within the robot workspace.

Remark 1: Consider that the system is initially inside the restricted zone; that is, $\tilde{d}(t) < 0$. In this case, Constraint 12 will be fulfilled only if $\dot{\tilde{d}}(t)$ is greater than zero, which means that the system will, at least, be pushed back to the boundary exponentially.

B. Maintaining the robot inside a safe region

Using the same reasoning as in Section IV-A, if we want to maintain the robot *inside* a safe region, we must redefine d_{safe} ; that is,

$$\tilde{d}(t) \triangleq d_{\text{safe}} - d(t),$$

with the final solution, assuming the desired error dynamics (12), given by

$$\mathbf{J}_d \dot{\mathbf{q}}_P - \mathbf{J}_d \dot{\mathbf{q}}_N + z_D = \eta_d \tilde{d}(t).$$

V. DISTANCE FUNCTIONS AND JACOBIANS FOR ACTIVE CONSTRAINTS

The proposed vector field inequality discussed in the previous section requires a distance function $d(t)$ and the corresponding distance Jacobian \mathbf{J}_d for each collidable pair. In this section, we find four distance functions and Jacobians for pairs in which one element is static and the second element is dynamic.

A. Point–static–plane distance Jacobian, $\mathbf{J}_{t,\pi}$

One of the primitives for virtual fixtures is the constraint of a point such that it is above a static plane. Given a reference frame \mathcal{F} , a plane π in dual quaternion space is given by [22]

$$\pi \triangleq \mathbf{n}_\pi + \varepsilon d_\pi,$$

in which $\mathbf{n}_\pi \in \mathbb{H}_p \cap \mathbb{S}^3$ is the normal to the plane and $d_\pi \in \mathbb{R}$ is the signed perpendicular distance between the plane and the origin of the reference frame. Moreover, the distance d_π is given by $d_\pi = \langle \mathbf{p}_\pi, \mathbf{n}_\pi \rangle$, where \mathbf{p}_π is an arbitrary point in the plane. If \mathcal{F}_π is a frame attached to the plane, the signed distance between \mathbf{t} , an arbitrary point in the robot kinematic chain, and the plane, from the point of view of the plane, is given by

$$d_{t,\pi}^\pi \triangleq \langle \mathbf{t}, \mathbf{n}_\pi \rangle - d_\pi. \quad (15)$$

The time derivative of (15) is

$$\frac{d(d_{t,\pi}^\pi)}{dt} \stackrel{(4)}{=} \langle \dot{\mathbf{t}}, \mathbf{n}_\pi \rangle = \underbrace{(\text{vec}_4 \mathbf{n}_\pi)^T}_{\mathbf{J}_{t,\pi}} \mathbf{J}_t \dot{\mathbf{q}}. \quad (16)$$

B. Line Jacobian, \mathbf{J}_{l_z}

The line Jacobian is a pre-requisite for the more complex Jacobians described in the following sections.

The Plücker line [22] $\underline{l}_z \in \mathcal{H}_p \cap \underline{\mathcal{S}}$ collinear to the z -axis of a frame represented by $\underline{\mathbf{x}} = \mathbf{r} + \varepsilon(1/2)\mathbf{t}\mathbf{r}$ is given by

$$\underline{l}_z = \mathbf{l}_z + \varepsilon \mathbf{m}_z, \quad (17)$$

where $\mathbf{l}_z = \mathbf{r} \hat{k} \mathbf{r}^*$ and $\mathbf{m}_z = \mathbf{t} \times \mathbf{l}_z$. The derivative of (17) is

$$\dot{\underline{l}}_z = \dot{\mathbf{l}}_z + \varepsilon \dot{\mathbf{m}}_z. \quad (18)$$

Hence,

$$\text{vec}_4 \dot{\underline{l}}_z \stackrel{(5)}{=} \underbrace{\left(\bar{\mathbf{H}}_4(\hat{k}\mathbf{r}^*) + \overset{+}{\mathbf{H}}_4(\mathbf{r}\hat{k}) \mathbf{C}_4 \right)}_{\mathbf{J}_{r_z}} \mathbf{J}_r \dot{\mathbf{q}} \quad (19)$$

in which $\mathbf{C}_4 = \text{diag}(1, -1, -1, -1)$. In addition,

$$\text{vec}_4 \dot{\mathbf{m}}_z = \underbrace{\frac{\left(\bar{\mathbf{H}}_4(\mathbf{l}_z) - \overset{+}{\mathbf{H}}_4(\mathbf{l}_z) \right) \mathbf{J}_t + \left(\overset{+}{\mathbf{H}}_4(\mathbf{t}) - \bar{\mathbf{H}}_4(\mathbf{t}) \right) \mathbf{J}_{r_z}}{2}}_{\mathbf{J}_{m_z}} \dot{\mathbf{q}}.$$

Finally, (18) can be re-written in term of joint velocities as

$$\text{vec}_8 \dot{\underline{l}}_z = \begin{bmatrix} \mathbf{J}_{r_z} \\ \mathbf{J}_{m_z} \end{bmatrix} \dot{\mathbf{q}} \triangleq \mathbf{J}_{l_z} \dot{\mathbf{q}}. \quad (20)$$

C. Line-static-point distance Jacobian, $\mathbf{J}_{l_z,p}$

The line-static-point Jacobian can be used to generate a remote center of motion. First, we notice that the distance between $\underline{l}_z \in \mathcal{H}_p \cap \underline{\mathcal{S}}$ and an arbitrary static point $\mathbf{p} \in \mathbb{H}_p$ is given by

$$d_{l_z,p} = \|\mathbf{p} \times \mathbf{l}_z - \mathbf{m}_z\|. \quad (21)$$

The derivative of (21) is

$$\begin{aligned} \dot{d}_{l_z,p} &= \frac{1}{d_{l_z,p}} \text{vec}_4(\mathbf{p} \times \mathbf{l}_z - \mathbf{m}_z)^T \text{vec}_4 \frac{d((\mathbf{p} \times \mathbf{l}_z - \mathbf{m}_z))}{dt} \\ &\stackrel{(20)}{=} \underbrace{\frac{1}{d_{l_z,p}} \text{vec}_4(\mathbf{p} \times \mathbf{l}_z - \mathbf{m}_z)^T (\bar{\mathbf{S}}(\mathbf{p}) \mathbf{J}_{r_z} - \mathbf{J}_{m_z})}_{\mathbf{J}_{l_z,p}} \dot{\mathbf{q}}. \end{aligned} \quad (22)$$

D. Point-static-line distance Jacobian, $\mathbf{J}_{t,l}$

The point-static-line Jacobian can be used to keep a point inside/outside a cylinder. First, we notice that the distance between an arbitrary line $\underline{l} \in \mathcal{H}_p \cap \underline{\mathcal{S}}$, such that $\underline{l} = \mathbf{l} + \varepsilon \mathbf{m}$, and a point $\mathbf{t} \in \mathbb{H}_p$ in the robot kinematic chain is given by

$$d_{t,l} = \|\mathbf{t} \times \mathbf{l} - \mathbf{m}\|. \quad (23)$$

The derivative of (23) is given by

$$\begin{aligned} \dot{d}_{t,l} &= \frac{1}{d_{t,l}} \text{vec}_4(\mathbf{t} \times \mathbf{l} - \mathbf{m})^T \text{vec}_4 \frac{d((\mathbf{t} \times \mathbf{l} - \mathbf{m}))}{dt} \\ &\stackrel{(4)}{=} \underbrace{\frac{1}{d_{t,l}} \text{vec}_4(\mathbf{t} \times \mathbf{l} - \mathbf{m})^T \bar{\mathbf{S}}(\mathbf{l})^T}_{\mathbf{J}_{t,l}} \mathbf{J}_t \dot{\mathbf{q}}. \end{aligned} \quad (24)$$

E. Line-static-line distance Jacobian

The line-static-line Jacobian is particularly useful for avoiding collisions between a moving cylinder and a static cylinder. In order to obtain the line-static-line Jacobian, we use the concept of dual angle between Plücker lines.

1) *Inner product Jacobian, $\mathbf{J}_{(\underline{l}_z, \underline{l})}$* : The dual cosine between Plücker lines $\underline{l}, \underline{l}_z \in \mathcal{H}_p \cap \underline{\mathcal{S}}$ is obtained by using the inner product [20]

$$\langle \underline{l}, \underline{l}_z \rangle = \underbrace{\|\underline{l}\|}_1 \underbrace{\|\underline{l}_z\|}_1 \cos(\phi + \varepsilon d_l) = \cos \phi - \varepsilon d_l \sin \phi, \quad (25)$$

where $d_l \in [0, \infty)$ and $\phi \in [0, 2\pi)$ are the distance and the angle between the lines, respectively.¹

Since the line \underline{l} is static, $\dot{\underline{l}} = 0$ and thus the derivative of (25) is given by

$$\begin{aligned} \text{vec}_8 \frac{d(\langle \underline{l}_z, \underline{l} \rangle)}{dt} &= - \underbrace{\frac{\left(\overset{+}{\mathbf{H}}_8(\underline{l}) + \bar{\mathbf{H}}_8(\underline{l}) \right)}{2}}_{\mathbf{J}_{(\underline{l}_z, \underline{l})}} \mathbf{J}_l \dot{\mathbf{q}} \\ \begin{bmatrix} \text{vec}_4 \dot{\mathcal{P}}(\langle \underline{l}_z, \underline{l} \rangle) \\ \text{vec}_4 \dot{\mathcal{D}}(\langle \underline{l}_z, \underline{l} \rangle) \end{bmatrix} &= \begin{bmatrix} \mathbf{J}_{\mathcal{P}(\underline{l}_z, \underline{l})} \\ \mathbf{J}_{\mathcal{D}(\underline{l}_z, \underline{l})} \end{bmatrix} \dot{\mathbf{q}}. \end{aligned} \quad (26)$$

2) *Cross product Jacobian, $\mathbf{J}_{\underline{l}_z \times \underline{l}}$* : Given the dual angle $\phi = \phi + \varepsilon d_l$, where $d_l \in [0, \infty)$ and $\phi \in [0, 2\pi)$, and the Plücker line $\underline{s} \in \mathcal{H}_p \cap \underline{\mathcal{S}}$, with $\underline{s} = \mathbf{s} + \varepsilon \mathbf{m}_s$, the cross product between \underline{l}_z and \underline{l} is given by [20]

$$\begin{aligned} \underline{l}_z \times \underline{l} &= \underbrace{\|\underline{l}_z\|}_1 \underbrace{\|\underline{l}\|}_1 \underline{s} \sin \phi \\ &= (\mathbf{s} + \varepsilon \mathbf{m}_s) (\sin \phi + \varepsilon d_l \cos \phi) \\ &= \mathbf{s} \sin \phi + \varepsilon (\mathbf{m}_s \sin \phi + \mathbf{s} d_l \cos \phi), \end{aligned} \quad (27)$$

in which \underline{s} is the line perpendicular to both \underline{l}_z and \underline{l} . The time derivative of the cross product between \underline{l}_z and the static

¹Given a function $f : \mathbb{D} \rightarrow \mathbb{D}$, where $\mathbb{D} \triangleq \{\mathbf{h} \in \mathcal{H} : \text{Im}(\mathbf{h}) = 0\}$, it is possible to show that $f(a + \varepsilon b) = f(a) + \varepsilon b f'(a)$. For more details, see [22].

line \underline{l} is

$$\text{vec}_8 \frac{d(\underline{l}_z \times \underline{l})}{dt} = \underbrace{\frac{(\bar{\mathbf{H}}_8(\underline{l}) - \mathbf{H}_8^+(\underline{l}))}{2}}_{\mathbf{J}_{\underline{l}_z \times \underline{l}}} \mathbf{J}_l \dot{\mathbf{q}}$$

$$\begin{bmatrix} \text{vec}_4 \dot{\mathcal{P}}(\underline{l}_z \times \underline{l}) \\ \text{vec}_4 \dot{\mathcal{D}}(\underline{l}_z \times \underline{l}) \end{bmatrix} = \begin{bmatrix} \mathbf{J}_{\mathcal{P}(\underline{l}_z \times \underline{l})} \\ \mathbf{J}_{\mathcal{D}(\underline{l}_z \times \underline{l})} \end{bmatrix} \dot{\mathbf{q}}. \quad (28)$$

3) *Distance Jacobian between non-parallel lines:* The distance $d_{\underline{l}_z, \underline{l}}$ between \underline{l}_z and \underline{l} when they are not parallel (i.e., $\phi \in (0, 2\pi) \setminus \pi$) can be obtained as

$$d_{\underline{l}_z, \underline{l}} = \frac{\|\mathcal{D}(\langle \underline{l}_z, \underline{l} \rangle)\|}{\|\mathcal{P}(\underline{l}_z \times \underline{l})\|} = \frac{\|d_l \sin \phi\|}{\|s_l \sin \phi\|} = d_l. \quad (29)$$

Noting that both the numerator and denominator of (29) are real numbers, we can find the derivative of (29) as

$$\dot{d}_{\underline{l}_z, \underline{l}} = \frac{1}{\underbrace{\|\mathcal{P}(\underline{l}_z \times \underline{l})\|}_a} \frac{d(\|\mathcal{D}(\langle \underline{l}_z, \underline{l} \rangle)\|)}{dt} - \frac{\underbrace{\|\mathcal{D}(\langle \underline{l}_z, \underline{l} \rangle)\|}_{b}}{\underbrace{\|\mathcal{P}(\underline{l}_z \times \underline{l})\|^2}_b} \frac{d(\|\mathcal{P}(\underline{l}_z \times \underline{l})\|)}{dt}. \quad (30)$$

We obtain the derivative of the norm of $\mathcal{D}(\langle \underline{l}_z, \underline{l} \rangle)$ using (3) and (26) as

$$\frac{d(\|\mathcal{D}(\langle \underline{l}_z, \underline{l} \rangle)\|)}{dt} = \frac{1}{\|\mathcal{D}(\langle \underline{l}_z, \underline{l} \rangle)\|} \underbrace{\text{vec}_4 \mathcal{D}(\langle \underline{l}_z, \underline{l} \rangle)^T \mathbf{J}_{\mathcal{D}(\langle \underline{l}_z, \underline{l} \rangle)}}_{\mathbf{J}_{\|\mathcal{D}(\langle \underline{l}_z, \underline{l} \rangle)\|}} \dot{\mathbf{q}} \quad (31)$$

and similarly we obtain the derivative of the norm of $\mathcal{P}(\underline{l}_z \times \underline{l})$ using (3) and (28) as

$$\frac{d(\|\mathcal{P}(\underline{l}_z \times \underline{l})\|)}{dt} = \frac{1}{\|\mathcal{P}(\underline{l}_z \times \underline{l})\|} \underbrace{\text{vec}_4 \mathcal{P}(\underline{l}_z \times \underline{l})^T \mathbf{J}_{\mathcal{P}(\underline{l}_z \times \underline{l})}}_{\mathbf{J}_{\|\mathcal{P}(\underline{l}_z \times \underline{l})\|}} \dot{\mathbf{q}}. \quad (32)$$

Finally, we substitute (31) and (32) in (30) to find

$$\dot{d}_{\underline{l}_z, \underline{l}} = \underbrace{\left(a \mathbf{J}_{\|\mathcal{D}(\langle \underline{l}_z, \underline{l} \rangle)\|} + b \mathbf{J}_{\|\mathcal{P}(\underline{l}_z \times \underline{l})\|} \right)}_{\mathbf{J}_{d_{\underline{l}_z, \underline{l}}}} \dot{\mathbf{q}}. \quad (33)$$

4) *Parallel distance Jacobian, $\mathbf{J}_{\underline{l}_z, \underline{l}}$:* In the degenerate case in which \underline{l}_z and \underline{l} are parallel (i.e., $\phi \in \{0, \pi\}$), the distance between them can be retrieved as

$$d_{\underline{l}_z, \underline{l}} \triangleq \|\mathcal{D}(\underline{l}_z \times \underline{l})\| = \|s d_l\| = d_l. \quad (34)$$

Resorting once more to (3), we find the derivative of (34) as

$$\dot{d}_{\underline{l}_z, \underline{l}} = \frac{1}{\|\mathcal{D}(\underline{l}_z \times \underline{l})\|} \underbrace{\text{vec}_4 (\mathcal{D}(\underline{l}_z \times \underline{l}))^T \mathbf{J}_{\mathcal{D}(\underline{l}_z \times \underline{l})}}_{\mathbf{J}_{d_{\underline{l}_z, \underline{l}}}} \dot{\mathbf{q}}. \quad (35)$$

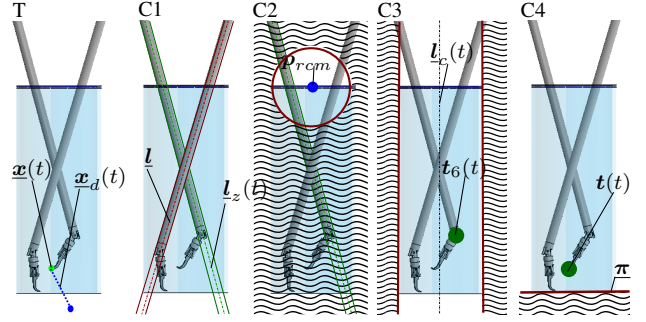


Fig. 2. Task and constraints used in the simulations. The task T consists of moving the end effector, $\underline{x}(t)$, of one of the tools in a given trajectory $\underline{x}_d(t)$. The constraints are: C1, a line-static-line distance constraint, to avoid collisions between tool shafts, where the shaft of the moving tool has a center-line given by $\underline{l}_z(t)$ and the static shaft has a center-line \underline{l} ; C2, a line-static-point distance constraint to generate the entry sphere with the center given by \mathbf{p}_{rcm} ; C3, a point-static-line distance constraint to prevent the lower part of the moving tool given by $\mathbf{t}_6(t)$ from colliding with the cylindrical workspace with center-line \underline{l}_c ; and C4, a point-static-plane distance constraint to prevent the end effector from crossing the lower bound of the cylindrical workspace given by the plane $\underline{\pi}$.

5) *Manipulator line-to-line distance Jacobian, $\mathbf{J}_{\underline{l}_z, \underline{l}}$:* The line-to-line distance Jacobian is given by combining (33) and (35) as

$$\mathbf{J}_{\underline{l}_z, \underline{l}} = \begin{cases} \mathbf{J}_{d_{\underline{l}_z, \underline{l}}} & \phi \in (0, 2\pi) \setminus \pi \\ \mathbf{J}_{d_{\underline{l}_z, \underline{l}}} & \phi \in \{0, \pi\} \end{cases}, \quad (36)$$

in which ϕ can be obtained as $\phi = \arccos \mathcal{P}(\langle \underline{l}, \underline{l}_z \rangle)$.

The distance between lines can be given by the composition of the distance (29) and (34) as

$$d_{\underline{l}_z, \underline{l}} = \begin{cases} d_{\underline{l}_z, \underline{l}} & \phi \in (0, 2\pi) \setminus \pi \\ d_{\underline{l}_z, \underline{l}} & \phi \in \{0, \pi\} \end{cases}. \quad (37)$$

VI. SIMULATIONS

In order to validate our approach,² we developed a realistic simulated version, using V-REP³ and DQ Robotics for MATLAB⁴, of a deep neurosurgical robotic system that we previously developed in close cooperation with neurosurgeons [4] (see Fig. 2). In deep neurosurgery, the workspace is highly constrained in the microscopic view. The diameter of the tools is 3.5 mm, and the radius and depth of the workspace cylinder are 2.8 cm and 8 cm, respectively.

In this preliminary evaluation, one of the tools was kept fixed while the second tool moved. Five simulations (S1-S5) with increasing complexity were run, as follows. S1: the task T consisted of moving the end effector along the desired trajectory with no virtual fixtures; S2: constraint C1 was added to prevent the shafts from colliding with each other using $\mathbf{J}_{\underline{l}_z, \underline{l}}$ from (37) and $d_{\underline{l}_z, \underline{l}}$ as in (37); S3: in addition to C1, a spherical entry-point constraint C2 was added to avoid collisions with the top part of the cylinder using $\mathbf{J}_{\underline{l}_z, p}$ from (22) and $d_{\underline{l}_z, p}$ as in (21); S4: in addition to constraints C1 and C2, a point line distance constraint C3 was added

²See accompanying video.

³<http://www.coppeliarobotics.com/>

⁴<http://dqrobotics.sourceforge.net>

to avoid collisions of the lower part of the shaft with the workspace boundary, which is represented by a cylinder, using $\mathbf{J}_{t,l}$ from (24) and $d_{t,l}$ as in (23); and finally, S5: in addition to constraints C1, C2, and C3, a point–static-plane distance constraint C4 was added to prevent the end effector from crossing the plane $\underline{\pi}$, using $\mathbf{J}_{t,\pi}$ from (16) and $d_{t,\pi}$ as in (15).

The robot has eight degrees-of-freedom in which the first, second, and fifth joints were prismatic and the remaining joints were revolute. The robots' initial configurations were such that the shafts were at a long distance from each other. The trajectory, which was the same for all simulations, was the screwlinear interpolation of four poses. The final form of the linear program, when all constraints were used, was

$$\begin{aligned} \min_{\mathbf{g}} & \left[-1^T \mathbf{J}_{\underline{x}} \ 1^T \mathbf{J}_{\underline{x}} \ 2 \cdot 1^T \mathbf{0}^T \ 0 \mid \mathbf{0}^T \mid 0 \ 0 \ 0 \ 0 \right] \mathbf{g} \\ \text{s.t.} & \begin{bmatrix} \mathbf{J}_{\underline{x}} & -\mathbf{J}_{\underline{x}} & -\mathbf{I} & \mathbf{I} & \mathbf{0} & \mathbf{0} & \mathbf{0} & \mathbf{0} & \mathbf{0} & \mathbf{0} \\ \mathbf{1}^T & \mathbf{1}^T & \mathbf{0}^T & \mathbf{0}^T & 1 & \mathbf{0}^T & 0 & 0 & 0 & 0 \end{bmatrix} \mathbf{g} = \begin{bmatrix} -\eta \text{vec}_8 \tilde{\underline{x}} \\ \beta \|\text{vec}_8 \tilde{\underline{x}}\|_1 \\ \mathbf{w}_l \\ \eta_{l_z,l} \tilde{d}_{C1} \\ \eta_{l_z,p} \tilde{d}_{C2} \\ \eta_{t,l} \tilde{d}_{C3} \\ \eta_{t,\pi} \tilde{d}_{C4} \end{bmatrix} \\ & \begin{bmatrix} \mathbf{W}_l & -\mathbf{W}_l & \mathbf{0} & \mathbf{0} & \mathbf{0} & \mathbf{0} & \mathbf{I} & \mathbf{0} & \mathbf{0} & \mathbf{0} \end{bmatrix} \mathbf{g} = \begin{bmatrix} \eta_{l_z,l} \tilde{d}_{C1} \\ \eta_{l_z,p} \tilde{d}_{C2} \\ \eta_{t,l} \tilde{d}_{C3} \\ \eta_{t,\pi} \tilde{d}_{C4} \end{bmatrix} \\ & \mathbf{g} \geq 0 \\ & \mathbf{g} = [\dot{\mathbf{q}}_P^T \ \dot{\mathbf{q}}_N^T \ \mathbf{y}^T \ z_A^T \ z_B^T \ z_l^T \ z_{C1} \ z_{C2} \ z_{C3} \ z_{C4}]^T, \end{aligned}$$

in which \mathbf{W}_l and \mathbf{w}_l are constraints for the joint limits [16], $z_l^T, z_{C1}, z_{C2}, z_{C3}, z_{C4}$ are slack variables, $\tilde{d}_{C1} = d_{\text{safe},C1} - d_{l_z,l}$, $\tilde{d}_{C2} = d_{l_z,p} - d_{\text{safe},C2}$, $\tilde{d}_{C3} = d_{t,l} - d_{\text{safe},C3}$, and $\tilde{d}_{C4} = d_{\text{safe},C4} - d_{t,\pi}$.

For all simulations, the trajectory tracking gain was $\eta = 50$, and $\beta = 40$. Whenever present in a given simulation, vector field inequality gains were set at the same value $\eta_{l_z,l} = \eta_{l_z,p} = \eta_{t,l} = \eta_{t,\pi} = 0.5$. The safety distances for each constraint were $d_{\text{safe},C1} = 5$ mm, $d_{\text{safe},C2} = d_{\text{safe},C3} = 14$ mm, and $d_{\text{safe},C4} = 0$.

VII. RESULTS AND DISCUSSION

The results of the simulation are shown in Fig. 3 in terms of the distance between shafts, the distance between the entry point and tool shaft, the distance between the lower point of the shaft and the cylinder centerline, and the distance between the tool tip and the lower plane.

Simulation S1, in which no virtual fixtures were applied caused collisions between the shafts and between the moving tool and the workspace boundaries. Constraining only the shafts in S2 was sufficient to avoid collisions between the shafts, but tool-boundary collisions still occurred. Constraining both the shafts and the entry point in S3 provided a collision-free shaft motion and prevented collisions with the uppermost part of the cylinder. Simulation S4 violated only the plane constraint, and S5 provided a collision-free path. From the point of view of trajectory error, as shown in Fig. 4, naturally S1 was able to follow the trajectory closely since no active constraints were applied. All other simulations presented tracking errors given the gradual imposition of

restrictions. The trajectories for all the experiments are shown in Fig. 5.

In S3, the robot showed a low amplitude vibration near the end of the trajectory, which may occur when the trajectory tracking error is unable to stabilize at the origin. It can be somewhat reduced by tuning β ; however, other solutions, such as regularizing the objective function, are being analyzed in ongoing research.

VIII. CONCLUSIONS

In this paper a novel method for applying active constraints using vector field inequalities was proposed. The method can be used to prevent a robot from entering a restricted zone or for maintaining its location inside a safe area, and is based on a Lyapunov stable solution that can handle both equality and inequality constraints. The vector field inequalities limit the velocity of the robot in the direction of the forbidden zone's boundary while leaving tangential velocities undisturbed. To use the method, a Jacobian describing the relation between the time derivative of the distance and joint velocities is required. In this work, four of the Jacobians are obtained for relations in which one of the entities is static. Simulation results for two eight-DOF neurosurgical arms showed that, by using the vector field inequalities and relevant primitives, all collisions could be avoided and the robot safely navigated through a restricted workspace.

The proposed method does not require a high-accuracy model of the environment, but the environment must be decomposed in sufficient primitives. However, it still requires high-accuracy calibration between the primitives and the robot. A practical methodology for achieving this is the topic of ongoing work. An additional topic of ongoing work is the tracking of a user generated trajectory, which raises points of discussion such as gain tuning for minimum trajectory tracking error and latency analysis. The implementation on the real platform is currently in progress.

REFERENCES

- [1] M. J. Lum, D. C. Friedman, G. Sankaranarayanan, H. King, K. Fodero, R. Leuschke, B. Hannaford, J. Rosen, and M. N. Sinanan, "The raven: Design and validation of a telesurgery system," *The International Journal of Robotics Research*, vol. 28, no. 9, pp. 1183–1197, 2009.
- [2] R. Taylor, P. Jensen, L. Whitcomb, A. Barnes, R. Kumar, D. Stoianovici, P. Gupta, Z. Wang, E. Dejuan, and L. Kavoussi, "A steady-hand robotic system for microsurgical augmentation," *The International Journal of Robotics Research*, vol. 18, no. 12, pp. 1201–1210, 1999.
- [3] A. Morita, S. Sora, M. Mitsuishi, S. Warisawa, K. Suruman, D. Asai, J. Arata, S. Baba, H. Takahashi, R. Mochizuki, *et al.*, "Microsurgical robotic system for the deep surgical field: development of a prototype and feasibility studies in animal and cadaveric models," *Journal of neurosurgery*, vol. 103, no. 2, pp. 320–327, 2005.
- [4] H. Ueda, R. Suzuki, A. Nakazawa, Y. Kurose, M. M. Marinho, N. Shono, H. Nakatomi, N. Saito, E. Watanabe, A. Morita, K. Harada, N. Sugita, and M. Mitsuishi, "Toward autonomous collision avoidance for robotic neurosurgery in deep and narrow spaces in the brain," *Procedia CIRP*, vol. 65, no. Supplement C, pp. 110 – 114, 2017. 3rd CIRP Conference on BioManufacturing.
- [5] M. Li, M. Ishii, and R. H. Taylor, "Spatial motion constraints using virtual fixtures generated by anatomy," *IEEE Transactions on Robotics*, vol. 23, no. 1, pp. 4–19, 2007.
- [6] B. Siciliano, L. Sciacivco, L. Villani, and G. Oriolo, *Robotics: Modelling, Planning and Control*. Advanced Textbooks in Control and Signal Processing, London: Springer-Verlag London, 2009.

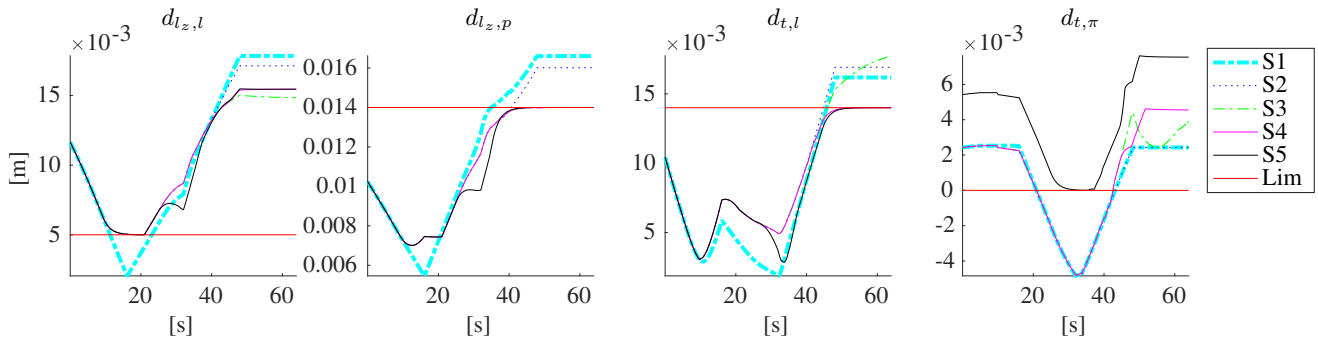


Fig. 3. Distance between collidable entities. Only S5 provided a collision-safe trajectory, since S4 violated the plane, S3 violated the plane and the lower part of the cylinder, S2 violated the plane and both the upper and lower parts of the cylinder, and S1 violated all constraints.

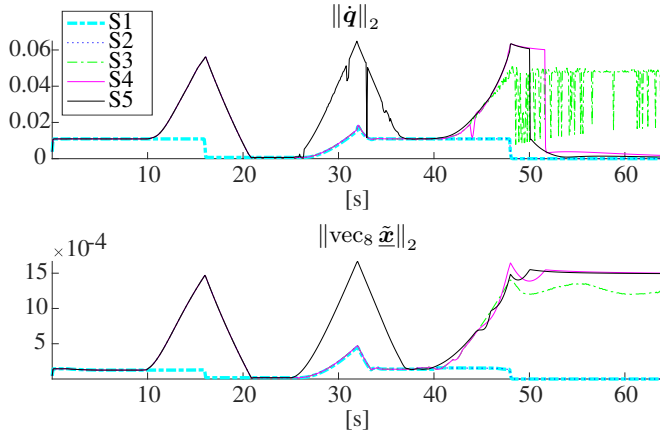


Fig. 4. Trajectory tracking error (bottom) and 2-norm of joint velocities (top). Only S1 could closely follow the prescribed trajectory as it had no active constraints. In all other simulations, some trajectory tracking error was allowed in order to avoid collisions.

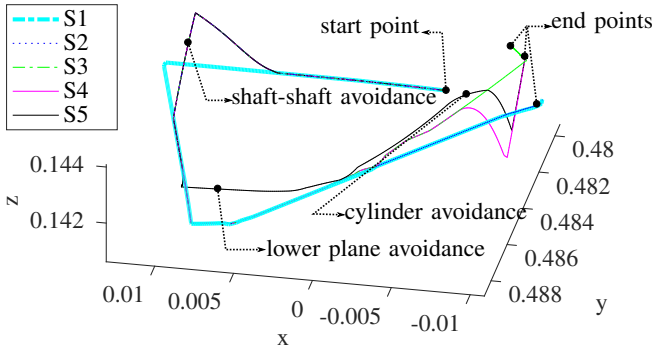


Fig. 5. Tool tip trajectories for all experiments. Notice that S1 is effectively the same as the desired trajectory, and S5 was the only collision-free trajectory.

[7] A. Kapoor, M. Li, and R. H. Taylor, “Constrained control for surgical assistant robots,” in *Robotics and Automation (ICRA), 2006 IEEE International Conference on*, pp. 231–236, 2006.

[8] N. Aghakhani, M. Geravand, N. Shahriari, M. Vendittelli, and G. Oriolo, “Task control with remote center of motion constraint for minimally invasive robotic surgery,” in *Robotics and Automation (ICRA), 2013 IEEE International Conference on*, pp. 5807–5812, IEEE, 2013.

[9] C. D. Pham, F. Coutinho, A. C. Leite, F. Lizaralde, P. J. From, and R. Johansson, “Analysis of a moving remote center of motion for robotics-assisted minimally invasive surgery,” in *Intelligent Robots and Systems (IROS), 2015 IEEE/RSJ International Conference on*,

pp. 1440–1446, IEEE, 2015.

[10] M. M. Marinho, M. C. Bernardes, and A. P. Bo, “Using general-purpose serial-link manipulators for laparoscopic surgery with moving remote center of motion,” *Journal of Medical Robotics Research*, vol. 1, no. 04, p. 1650007, 2016.

[11] S. A. Bowyer, B. L. Davies, and F. R. y Baena, “Active constraints/virtual fixtures: A survey,” *IEEE Transactions on Robotics*, vol. 30, no. 1, pp. 138–157, 2014.

[12] Z. Chen, A. Malpani, P. Chalasani, A. Deguet, S. S. Vedula, P. Kazanzides, and R. H. Taylor, “Virtual fixture assistance for needle passing and knot tying,” in *Intelligent Robots and Systems (IROS), 2016 IEEE/RSJ International Conference on*, pp. 2343–2350, IEEE, 2016.

[13] M.-A. Vitrani, C. Poquet, and G. Morel, “Applying virtual fixtures to the distal end of a minimally invasive surgery instrument,” *IEEE Transactions on Robotics*, vol. 33, no. 1, pp. 114–123, 2017.

[14] J. Funda, R. H. Taylor, B. Eldridge, S. Gomory, and K. G. Gruben, “Constrained cartesian motion control for teleoperated surgical robots,” *IEEE Transactions on Robotics and Automation*, vol. 12, no. 3, pp. 453–465, 1996.

[15] V. M. Gonçalves, P. Fraise, A. Crosnier, and B. V. Adorno, “Parsimonious kinematic control of highly redundant robots,” *IEEE Robotics and Automation Letters*, vol. 1, no. 1, pp. 65–72, 2016.

[16] J. J. Quiroz-Omaña and B. V. Adorno, “Whole-Body Kinematic Control of Nonholonomic Mobile Manipulators Using Linear Programming,” *Journal of Intelligent & Robotic Systems*, in press.

[17] T. Xia, C. Baird, G. Jallo, K. Hayes, N. Nakajima, N. Hata, and P. Kazanzides, “An integrated system for planning, navigation and robotic assistance for skull base surgery,” *The International Journal of Medical Robotics and Computer Assisted Surgery*, vol. 4, no. 4, pp. 321–330, 2008.

[18] R. Prada and S. Payandeh, “On study of design and implementation of virtual fixtures,” *Virtual reality*, vol. 13, no. 2, pp. 117–129, 2009.

[19] B. V. Adorno, *Two-arm Manipulation: From Manipulators to Enhanced Human-Robot Collaboration [Contribution à la manipulation à deux bras : des manipulateurs à la collaboration homme-robot]*. PhD Dissertation, Université Montpellier 2, 2011.

[20] A. T. Yang, *Application of quaternion algebra and dual numbers to the analysis of spatial mechanisms*. PhD thesis, Columbia University, 1963.

[21] A. Perez and J. M. McCarthy, “Dual Quaternion Synthesis of Constrained Robotic Systems,” *Journal of Mechanical Design*, vol. 126, no. 3, pp. 425–435, 2004.

[22] B. V. Adorno, “Robot kinematic modeling and control based on dual quaternion algebra — Part I: Fundamentals,” 2017.

[23] J. M. Selig, *Geometric fundamentals of robotics*. Springer-Verlag New York Inc., 2nd ed., 2005.

[24] B. V. Adorno, P. Fraise, and S. Druon, “Dual position control strategies using the cooperative dual task-space framework,” in *Intelligent Robots and Systems (IROS), 2010 IEEE/RSJ International Conference on*, pp. 3955–3960, IEEE, 2010.

[25] A. Escande, N. Mansard, and P.-B. Wieber, “Hierarchical quadratic programming: Fast online humanoid-robot motion generation,” *The International Journal of Robotics Research*, vol. 33, pp. 1006–1028, may 2014.